

The Electron-Phonon Coupling Constant for Single-Layer Graphene on Metal Substrates Determined from He Atom Scattering

G. Benedek^{a,b}, J. R. Manson^{a,c} and S. Miret-Artés^{a,d}

^a Donostia International Physics Center (DIPC), Paseo Manuel de Lardizabal, 4, 20018 Donostia-San Sebastian, Spain

^b Dipartimento di Scienza dei Materiali, Università di Milano-Bicocca, Via Cozzi 55, 20125 Milano, Italy

^c Department of Physics and Astronomy, Clemson University, Clemson, South Carolina 29634, USA

^d Instituto de Física Fundamental, Consejo Superior de Investigaciones Científicas, Serrano 123, 28006 Madrid, Spain

E-mail:

giorgio.benedek@unimib.it, jmanson@clemson.edu, s.miret@iff.csic.es

June 27, 2020

Abstract. Recent theory has demonstrated that the value of the electron-phonon coupling strength λ can be extracted directly from the thermal attenuation (Debye-Waller factor) of Helium atom scattering (HAS) reflectivity. This theory is here extended to multivalley semimetal systems and applied to the case of graphene on different metal substrates and graphite. It is shown that λ rapidly increases for decreasing graphene-substrate binding strength. The method is suitable for analysis and characterization of not only the graphene overlayers considered here, but also other layered systems such as twisted graphene bilayers. We predict $\lambda_{HAS} = 0.89 \pm 0.04$ for the hypothetical flat free-standing graphene with cyclic boundary conditions. The overall uncertainty in the derived values of λ_{HAS} is estimated to be of the order of 10% or less.

1. Introduction

Current interest in single-layer graphene supported on metal substrates has led several experimental groups to investigate a number of such systems with He atom scattering (HAS), [1, 2, 3, 5, 6, 7, 8, 9, 9, 10, 11, 12] as well as the surface of clean highly ordered pyrolytic graphite (HOPG) graphite, C(0001).[1, 2, 3] Two of these systems, namely graphene (Gr) on Ni(111) and Gr/Ru(111) have also been investigated with Ne atom scattering. [10, 11] In all of these systems high quality data are available for the thermal attenuation of the specular diffraction peak over a large range of temperatures. Such thermal attenuation measurements are interesting because it has been shown that they

can be used to extract values of the electron-phonon coupling constant λ (also known as the mass correction factor) in the surface region.

The ability of atom scattering to measure λ relies on the fact that colliding atoms are repelled by the surface electron density arising from electronic states near the Fermi level, and energy is exchanged with the phonon gas primarily via the electron-phonon coupling. The electron-phonon coupling constant λ at the surface is defined as the average $\lambda = \langle \lambda_{\mathbf{Q},\nu} \rangle = \sum_{\mathbf{Q},\nu} \lambda_{\mathbf{Q},\nu} / N$ over the contributions $\lambda_{\mathbf{Q},\nu}$ coming from all the individual phonon modes, where \mathbf{Q} is the phonon parallel wave vector, ν the branch index, and N is the total number of phonon modes. [13]

It has been theoretically demonstrated that the intensity of peak features due to specific (\mathbf{Q}, ν) phonon modes as observed in inelastic He atom scattering spectra are individually proportional to their corresponding $\lambda_{\mathbf{Q},\nu}$. [14, 15] This prediction has been verified through detailed comparisons of calculations with experimental He scattering measurements of multiple layers of Pb on a Cu(111) substrate. [14, 15] Since the thermal attenuation of any quantum peak feature in the atom scattering spectra is due to an average over the mean square displacement of all phonon modes weighted by the respective electron-phonon coupling, it is not surprising that such attenuation can be related to the average $\lambda_{HAS} = \langle \lambda_{\mathbf{Q},\nu} \rangle$. [16, 17, 18, 19] This will be discussed in more detail below in Section 2 where the theory is briefly outlined. In Section 3 values of λ_{HAS} are obtained from the available He atom scattering data on C(0001). Section 4 presents an analysis of λ_{HAS} from the available data on Gr adsorbed on close-packed metal substrates by analyzing the thermal attenuation of the specular He atom scattering peaks. It is shown that the λ_{HAS} values exhibit an interesting relationship when compared with the relative binding strengths of the graphene to the corresponding metal substrate. Finally, in the Supplementary Material (see Appendix), a discussion is presented of the shear-vertical (ZA) mode of substrate-supported thin layers such as Gr/metals, and how it compares to the flexural mode of a thin flake of the same unsupported two dimensional (2D) material with free-boundary conditions. A summary and a few conclusions are drawn in Section 5 at the end of this work.

2. Theory

As a function of the temperature T , the thermal attenuation of quantum features in He atom spectra, such as elastic diffraction observed in angular distributions and the diffuse elastic peak observed in energy-resolved spectra, is given by a Debye-Waller (DW) factor. [20, 21, 22, 23] This is expressed as a multiplicative factor $\exp\{-2W(\mathbf{k}_f, \mathbf{k}_i, T)\}$ where \mathbf{k}_i and \mathbf{k}_f are the incident and final wave vectors of the He atom projectile. This means that the intensity of any elastic peak is given by

$$I(T) = I_0 \exp\{-2W(\mathbf{k}_f, \mathbf{k}_i, T)\}, \quad (1)$$

where I_0 is the intensity the peak would have at $T = 0$ in the absence of zero-point motion (rigid lattice limit). In general $I_0 > I(0)$.

The DW exponent is expressed by $2W(\mathbf{k}_f, \mathbf{k}_i, T) = \langle (\Delta\mathbf{k} \cdot \mathbf{u}^*)^2 \rangle_T$, where $\Delta\mathbf{k} = \mathbf{k}_f - \mathbf{k}_i$ is the scattering vector, \mathbf{u}^* is the effective phonon displacement felt by the projectile atom upon collision, and $\langle \dots \rangle_T$ denotes the thermal average. However, He atom scattering experiments typically use energies below 100 meV. The atoms do not penetrate the surface, and in fact are exclusively scattered by the surface electron density a few Å above the first layer of atomic cores. Thus the exchange of energy through phonon excitation occurs via the phonon-induced modulation of the surface electron gas; in other words via the electron-phonon (e-ph) interaction. This implies that the effective displacement \mathbf{u}^* is not that of the atom cores, such as would be measured in a neutron or X-ray diffraction experiment, but is the phonon-induced displacement of the electron distribution outside the surface at the classical turning point where the He atom is reflected.[16, 18] However, the effective mean square displacement of the electron density is related directly to that of the atom cores and shares many of its properties. Notably, for a crystal obeying the harmonic approximation and for sufficiently large temperature (typically temperatures comparable to or greater than the Debye temperature) $\langle (\Delta\mathbf{k} \cdot \mathbf{u}^*)^2 \rangle_T$ is to a very good approximation linear in T , and the proportionality between λ_{HAS} and the DW exponent, for the simplest case of specular diffraction, reads as [16]

$$2W(\mathbf{k}_f, \mathbf{k}_i, T) = 4\mathcal{N}(E_F) \frac{mE_{iz}}{m_e^*\phi} \lambda_{HAS} k_B T, \quad (2)$$

where $\mathcal{N}(E_F)$ is the electronic density of states (DOS) per unit cell at the Fermi energy E_F , m_e^* is the electron effective mass, ϕ is the work function, m is the projectile atomic mass and k_B is the Boltzmann constant. The quantity $E_{iz} = E_i \cos^2(\theta_i) = \hbar^2 k_{iz}^2 / 2m$ is the incident energy associated with motion normal to the surface at the given incident angle θ_i . For application to non-specular diffraction peaks or to other elastic features Eq. (2) should be adjusted to account for the correct scattering vector appropriate to the experimental scattering configuration, namely $4k_{iz}^2 \rightarrow \Delta\mathbf{k}^2 = (\mathbf{k}_f - \mathbf{k}_i)^2$.

Given the form of Eq. (2) it is useful to define the dimensionless quantity n_s as

$$n_s = \frac{\pi\hbar^2\mathcal{N}(E_F)}{m_e^*a_c}, \quad (3)$$

where a_c is the area of a surface unit cell. With this definition and the help of Eqs. (1) and (2) the following form for λ_{HAS} is obtained

$$\lambda_{HAS} = \frac{\pi}{2n_s} \alpha; \quad \alpha \equiv \frac{\phi \ln[I(T_1)/I(T_2)]}{a_c k_{iz}^2 k_B (T_2 - T_1)}, \quad (4)$$

where T_1 and T_2 are any two temperatures in the linearity region. Eq. (4) neatly separates the surface electronic properties from the quantities measured in an actual experiment. The electronic properties expressed by the ratio $\mathcal{N}(E_F)/m_e^*$ are contained in the dimensionless n_s , while the readily determined work function of the surface and the experimentally measured slope of the DW exponent are in α .

In the case of supported graphene there is certain amount of charge transfer to and from the Dirac cones, depending on the difference between the work function of

graphene and that of the substrate. The work function of self-standing graphene of 4.5 eV is smaller than that of metal surfaces considered here. [24] Therefore they should all act as acceptors. Angle resolved photoelectron scattering (ARPES) data show, however, that Ir(111) (H. Vita *et al.*), [25] Pt(111) (P. Sutter *et al.*), [26] and Ni(111) (A. Alattis *et al.*), [27] act as acceptors with respect to graphene, whereas Ru(0001) (Katsiev *et al.*), [28] and Cu(111) (Walter *et al.*) [29] act as donors. Former HAS studies on Gr/Ru(0001) have provided evidence that the tail of the substrate electron charge density actually extends beyond the graphene. [8] Thus the substrate surface work function has been used in Eq. (4), its role being to account for the steepness of the He-surface repulsive potential within the WKB approximation. [16, 18] In either electron or hole doping each Dirac cone contributes a DOS at the Fermi level, $\mathcal{N}(E_F) = a_c k_F / \pi \hbar^2 v_F^2$, with k_F the Fermi wavevector referred to a K-point of the surface Brillouin zone (SBZ), and v_F the Fermi velocity. By identifying m_e^* with the cyclotron effective mass for doped graphene $m_e^* = \hbar k_F / v_F$, [30] this gives $n_s = 1$ for a single Dirac cone. Although only one third of a cone is within the SBZ, so that diametric electron transitions at the Fermi level connect points in neighboring SBZs, the latter are equivalent to umklapp transitions with \mathbf{G} vectors in the Γ M directions between different cone thirds inside the SBZ (umklapp intervalley transitions). With the inclusion of these transitions, $n_s = 6$ is the appropriate value.

It is noted however that these transitions couple to phonons near the zone center and give therefore a modest contribution to λ . A thorough ARPES study by Fedorov *et al.* of graphene on Au(111), doped with alkali and Ca donor impurities, and electron concentrations ranging from $2 \cdot 10^{14}$ (for Cs) to $5 \cdot 10^{14}$ electrons/cm² (for Ca), shows that the major contribution to λ actually comes from phonons near the zone boundaries KMK'. [31] The derived Eliashberg function, providing the e-ph-weighed phonon DOS projected onto the impurity coordinates exhibits resonances with graphene phonons whose wavevectors arguably correspond to good Fermi surface nestings. The fact that the separation between the ZA and the optical phonon peaks increases with doping from that for Cs, near the K-point, to the one at smaller wavevectors for the largest Ca doping suggests that the e-ph coupling is mostly due to KK' intervalley transitions, either direct along the six edges (thus counting 3) or umklapp along the three long diagonals. First principle calculations by Park *et al.* appear to confirm the role of these transitions. [32] This is just the intervalley e-ph coupling mechanism introduced by Kelly and Falicov in the 1970s for charge density wave transitions in semiconductor surface inversion layers. [33, 34, 35] In this case $n_s = 6$ enumerates the different nesting conditions contributing to the e-ph coupling strength λ , and is here adopted for graphene and graphite, independently of whether they are electron- or hole-doped.

3. Graphite

Clean graphite C(0001) presents a weakly corrugated surface potential to He atom scattering which means that the specular peak is the dominant elastic scattering feature.

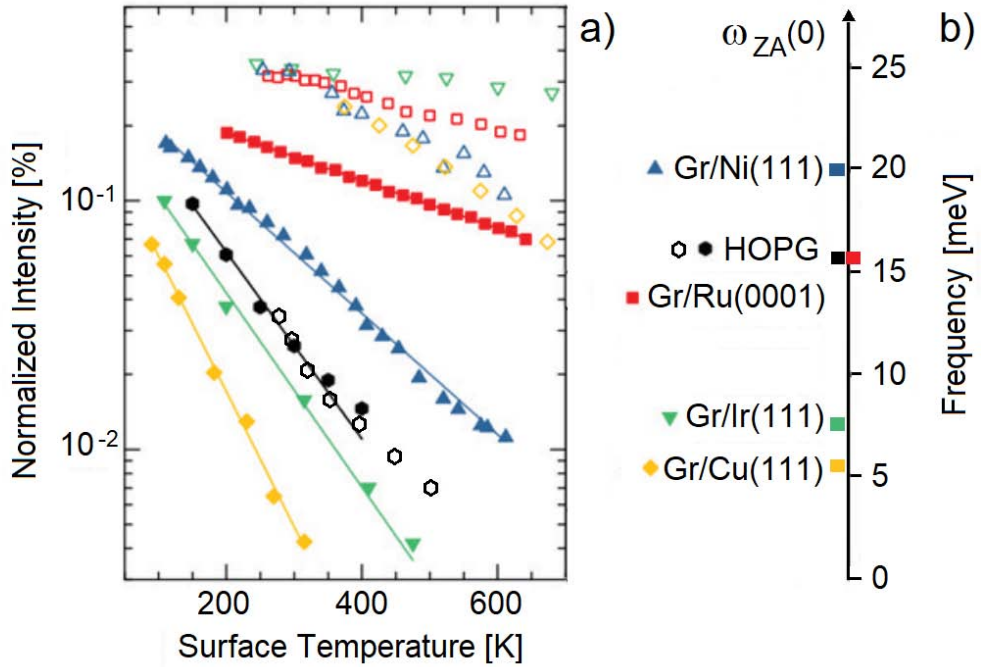


Figure 1. a) The normalized specular HAS intensity in log scale (proportional to the DW exponent) as a function of temperature for several systems of single-layer graphene supported on metal substrates (full symbols, defined in panel b)), together with similar data for the clean metals (open symbols). Also shown are the data for HOPG graphite at low (full hexagons [1]) and high temperature (open hexagons [36]). b) The ZA mode frequency at $\mathbf{Q} = 0$ for HOPG graphite and the Gr/metal systems shown in panel a). The data are from Ref. [1] with some adjustment as explained in the text.

The thermal attenuation of C(0001) has been measured by three independent groups over temperatures ranging from below 150 K to 500 K. [1, 2, 3, 36] As is apparent from the plots of the DW exponent in Fig. 1a), measured for graphite as a function of T by Oh *et al.* [2] and by Vollmer [36], the slope is essentially linear at lower temperature up to about 350 K. The slopes of the different measurements, and using $n_s = 6$, provide the values of λ_{HAS} listed in Table 1 together with the input parameters and the respective references. The average over the available data gives for graphite $\lambda_{HAS} = 0.36 \pm 0.04$. In general, the uncertainty in the slopes of the DW plot is not the only uncertainty in these calculations, because uncertainties in other parameters extracted from the literature are not always given. However, our estimation is that the overall uncertainty on λ_{HAS} is around 10% or less.

As is seen in Fig. 1a), above 350 K the slope of $2W(T)$ clearly decreases, apparently tending to a value about a factor of 2 smaller at high temperature, and so does λ_{HAS} . This behavior is very interesting and is probably the consequence of the gradual transition of graphite from negative to positive in-plane thermal expansion, occurring at ~ 500 K. [37, 38] A bond contraction, like that produced by an external pressure, generally yields a larger λ , while a dilation means a smaller λ , with similar consequences

on the superconducting critical temperature T_c . [39] This may explain the transition with temperature from a larger to a smaller λ_{HAS} observed in graphite. Interestingly, this is not observed in graphene, where the in-plane thermal expansion is predicted to remain negative up to a considerably larger temperature, well above the temperature range so far considered in HAS experiments. [40] It is seen from the last column in Table 1 that there is a rather large range of reported values of λ for bulk graphite, so that the values of λ_{HAS} at the surface as measured by He atom scattering are well within the range of reported bulk values.

4. Graphene on Metal Substrates

All of the systems of single layer graphene supported on close-packed metal surfaces for which DW plots of the specular diffraction peak have been measured are listed in Table 1. For two of these systems, Gr/Ni(111) and Gr/Ru(0001), measurements were made with both He and Ne atom scattering. For Gr/Ni(111), in addition to experiments done with He and Ne atoms, measurements were taken at very low incident energy using the ^3He isotope.

In all experiments atom diffraction and diffuse elastic scattering measurements provide accurate control of the surface long-range order and defect concentrations, respectively, which ensures a high quality of the graphene-substrate interface. The input parameters needed for evaluating λ_{HAS} are given in Table 1 together with the relevant references. For several of the clean metals λ_{HAS} has also been independently determined and those values appear in the next-to-last column. As stated previously for the case of graphite, the final column gives values measured for the e-ph constant λ of the pure bulk metal. There is a significant amount of spread in the reported values for the bulk metals, but the values of λ_{HAS} derived here for Gr/metals compare favorably. It is also interesting to note that the values of λ_{HAS} are quite similar regardless of whether the projectile is He or Ne. The value 0.16 obtained for Gr/Ni(111) using Ne atoms or very low energy (8 meV) ^3He atoms with the spin-echo detection technique is close to that of ^4He at the much larger energy of 66 meV which is 0.19.

It is of interest to compare the values of λ_{HAS} calculated here with the bonding strength of the graphene to these metals. The Gr/metal bonding strength is usually judged by the Gr-metal separation distance, and the systems that have been investigated fall into two different categories, weakly bonded with a separation distance greater than 3 Å and strongly bonded whose separation distance is 2.5 Å or less. Among the former are the close packed surfaces of Ag, Au, Cu, Pt and Ir, while the latter examples include Pd, Rh, Ru Ni, Co and Re. [41] Another way of evaluating bonding strengths is by comparing the frequencies $\omega_{ZA}(0)$ of the shear vertical ZA mode at the zone center at parallel wavevector $\mathbf{Q} = 0$. At long wavelengths the ZA mode is nearly dispersionless as a function of \mathbf{Q} for small \mathbf{Q} and acts like an Einstein mode with a spring constant $f_\perp = M^* \omega_{ZA}^2(0)$ where $M^* = 2M_C M_S / (2M_C + M_S)$ is the effective mass, M_C the carbon mass and M_S is the mass of the substrate atom. For graphite M_S coincides with the

Table 1. The mass enhancement factor λ_{HAS} obtained from atom scattering data for HOPG graphite and single-layer graphene adsorbed on metal crystal substrates is shown in the column marked as λ_{HAS}/Gr . All measurements were done with ordinary HAS, except where otherwise noted in the first column. All values of λ_{HAS} for Gr/metals were derived using $n_s = 6$, and are calculated using the unit cell area a_c of the metal substrate. The column marked as “ $\lambda_{HAS}/\text{substrate}$ ” gives the values determined for the clean metal substrate surface. (Values of other parameters showing no error indication are taken from the literature, where possible error sources are discussed. [42, 43, 44, 45, 46, 47]) A theoretical calculation by Park *et al.* produces a value of up to $\lambda = 0.21$ for single-layer free-standing graphene, depending on doping level.[32]

Surface	T [K]	E_i [meV]	ϕ [eV]	α	λ_{HAS} Gr	λ_{HAS} substrate	λ (substrate bulk values)
C(0001)	150-400 [2, 1]	63	4.5 [49]	1.70	0.41		0.70±0.08 [48]
	250-360 [36]	69		1.41	0.37		0.034-0.28 [32]
	400-500 [36]	69		0.76	0.20		≤ 0.20 [50]
	300-360 [3]	63		1.76	0.46		
Gr/Ni(111) (³ He atoms) (Neon atoms)	200-400 [11, 1]	66	5.35 [44]	0.71	0.19	0.56	0.3, 0.7 [46]
	200-700 [12]	8		0.69	0.16	0.36	
	100-200 [11]	66		0.58	0.16		
Gr/Ru(0001) (Neon atoms)	300-400 [3]	67	4.71 [44]	0.44	0.14	0.44	0.45 [45]
	200-600 [9]	32		0.38	0.15	0.33	0.4 [43]
	90-150 [9]	43		0.58	0.18	0.39	
Gr/Ir(111)	100-500 [1]	17.5	5.76 [44]	1.88	0.54	0.30	0.41 [46], 0.34 [42] 0.50 [45]
Gr/Rh(111)	150-450 [6]	19.3 63	4.98 [44]	1.65 1.16	0.43 0.31		0.41, 0.51 [46]
Gr/Pt(111)	300-400 [3]	67	5.70 [44]	1.53	0.54		0.66 [46]
Gr/Cu(111)	100-300 [1]	28	4.98 [44]	2.56	0.69	0.083	0.093[47], 0.13 [45] 0.1 [43]

planar unit cell mass $2M_C$ and therefore $M^* = M_C$. Figure 2 shows λ_{HAS} plotted as a function of the spring constant f_\perp . Values of $\omega_{ZA}(0)$ measured by HAS are taken from Refs. [1] and [41], except for that of Gr/Pt(111), extrapolated from Politano *et al.* high resolution electron energy loss spectroscopy (HREELS) data. [51]

Figure 2 shows a clear and interesting correlation between λ_{HAS} and the graphene-substrate interaction: the weaker is this interaction, the stronger is the e-ph coupling in graphene. This may be qualitatively understood by considering that a stronger interaction with the substrate implies a substantial reduction of the vertical mean square displacement, and possibly also some localization of graphene free electrons.

Some comments are in order about two of the values of $\omega_{ZA}(0)$ for the ZA mode that have been reported in the literature. In the case of Gr/Ru(0001) two widely different

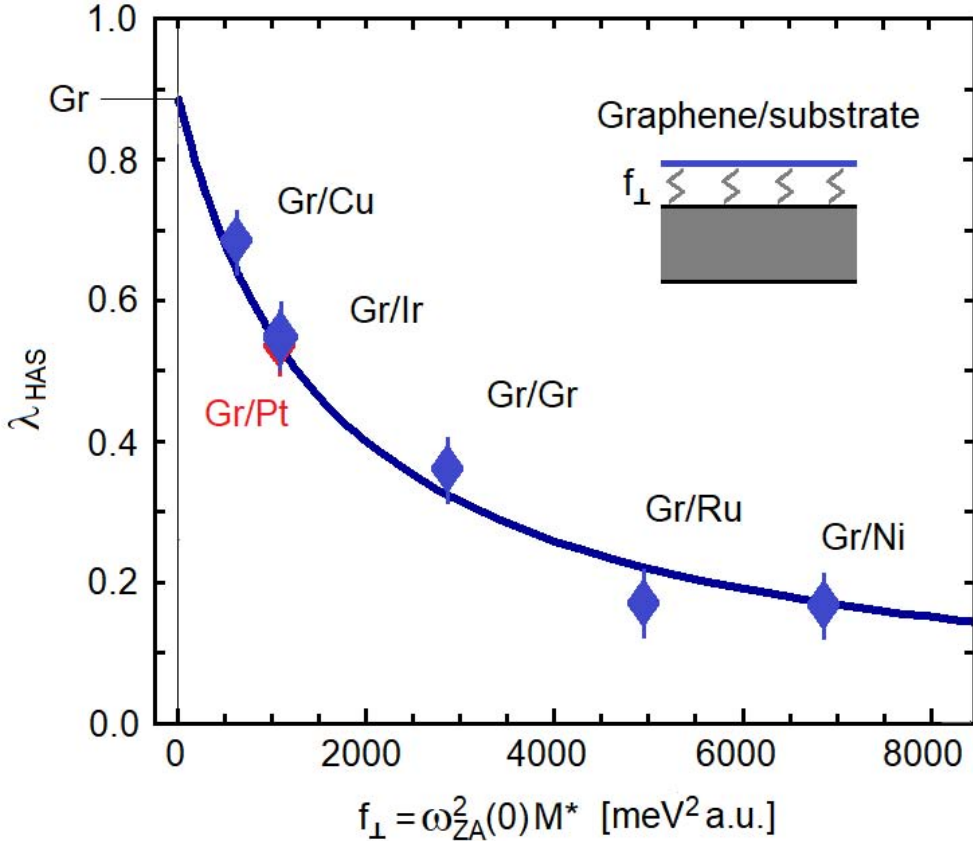


Figure 2. The mass enhancement factor λ_{HAS} plotted as a function of the ZA mode spring constant f_{\perp} , coupling graphene to the substrate, where M^* is the carbon dimer-substrate atom effective mass in atomic units (a.u.). The data are from Ref. [41], with some adjustment, and the data point for Gr/Rh(111) [6] is not included; see discussion in the text. The value of $\omega_{ZA}(0)$ for Gr/Pt(111) has been extrapolated from Politano *et al.* HREELS data. [51] The fitting curve, as explained in the text, allows the extrapolation of the value $\lambda = 0.89 \pm 0.04$ for the ideally flat self-standing graphene (error bar calculated from the mean-square relative deviation from the fitting curve).

values of 16 and 27 meV have been reported. [8, 41, 52] The value of 16 meV was measured by HAS over a range of parallel wavevector \mathbf{Q} that clearly demonstrates its dispersion behaving quadratically at large \mathbf{Q} as expected (see discussion below and supplementary material). The value of 27 meV measured with HREELS [52] appears to be incorrectly assigned. The reason for this assessment is that this mode also appears in HREELS measurements of the clean Ru(0001) surface, although at the slightly higher energy of a little over 30 meV (at the Γ point) where it is identified as the optical mode S_2 . [53, 54] The reason for the small energy difference between 27 and 30 meV can be explained by the fact that the tightly bound Gr simply weights down the outermost Ru layer, giving it a slightly smaller energy. Thus, it appears that the value of 27 meV for Gr/Ru(0001) should be assigned to the S_2 mode and not to the ZA mode. In Fig. 2 the

value $\omega_{ZA}(0) = 16$ meV has been used.

Another reported value of $\omega_{ZA}(0)$ that needs to be discussed is that of Gr/Rh(111) for which a value of 7 meV has been reported. [6] This value would appear to be too small when compared with the other strongly bound Gr/metal systems such as Gr/Ni and Gr/Ru where the value is rather in the range of 16 - 20 meV. Moreover, no upward dispersion is apparently observed, as would be expected. It is unfortunate that no phonon measurements were reported above 12 meV for this system. Other HAS measurements, for example for Gr/Ru(0001) and Gr/Ni(111) have shown that there are a variety of other modes and features that can produce peaks in the energy-resolved spectra at energies below 10 meV, including backfolding of the Rayleigh mode due to the super-periodicity of the moiré patterns induced on these strong binding graphene layers. [8, 9] In spite of this caveat about $\omega_{ZA}(0)$ for Gr/Rh(111), the corresponding value of $\lambda = 0.43$ for $f_{\perp} = 954 \text{ meV}^2 \text{ a.u.}$ is not far from fitting into the observed λ_{HAS} vs. f_{\perp} correlation. Since the phonon mean square displacement is inversely proportional to the Debye effective force constant f_D , it is reasonable to suggest that λ for the supported graphene should then scale as $A/(f_D + f_{\perp})$ with A a constant and f_D chosen to be the value of f_{\perp} for self-standing graphene. The fit with this scaling and $f_D = 1650 \text{ meV}^2 \text{ a.u.}$ is quite reasonable, as seen in Fig. 2, and gives a prediction of $\lambda_{HAS} = 0.89 \pm 0.04$ for the hypothetical flat free-standing graphene with cyclic boundary conditions.

The λ_{HAS} values reported in Table 1 fall in the same range as those reported by Fedorov *et al.* for electron-doping, [31] although the doping mechanism is different, one being achieved by changing the substrate, the other by changing the impurities. In both cases, however, λ increases with the softening of an acoustic mode, whether respectively due to the ZA mode dependence on the force constant f_{\perp} between graphene and the substrate, or to the same graphene ZA mode in resonance with the impurity-induced mode. Note that in the Fedorov *et al.* experiments [31] the Cs and Ca doping levels mentioned above respectively correspond to about 0.05 and 0.13 electrons per C atom, which are in the range of present substrate-graphene charge transfers. Despite these similarities it should be noted that the impurity contribution to the Fermi level DOS is sufficiently low and can be neglected, whereas the substrate contribution can be relevant. In the extreme weak-coupling limit, unquenched substrate surface states can exist at the Fermi level, with an additional contribution to that of Dirac cones. The model parameter suitable to incorporate these contributions is n_s , which may then be greater than 6. It is therefore likely that the value of λ_{HAS} reported for Gr/Cu(111) in Table 1 and Fig. 2 is overestimated. Actually it should be noted that all the values of λ_{HAS} reported in Table 1 for weakly bonded graphene systems are much larger than the values for a graphene single layer as calculated by Park *et al.* even at comparatively large doping levels ($\lambda < 0.21$), [32] although consistent with values from recent studies on n-doped graphene discussed in the following paragraphs.

The possibility of increasing λ with doping has stimulated several recent studies, all aiming at high- T_c superconductivity in graphene. Just two examples are the analysis by Zhou *et al.* on heavily N-(electron) and B-(hole) doped graphene, [55]

and the remarkable transport properties reported by Larkins *et al.* in phosphorous-doped graphite and graphene, apparently suggesting the onset of superconductivity at temperatures as high as 260 K. [56] Among graphene systems where superconductivity is induced by the contact with a periodic Ca layer and the consequent addition of a 2D electron gas at the Fermi level, worth mentioning are the works by Yang *et al.* where interband electron-phonon coupling is shown to play an important role, [57] and by Chapman *et al.* on Ca-doped graphene laminates. [58] Similarly, electron-doped material such as Li-covered graphene has also been predicted from first-principle calculations to attain a λ value as large as 0.61 with a superconducting $T_c = 8.1$ K. [59]

Another way to induce superconductivity in graphene is the proximity effect, occurring, as demonstrated by Di Bernardo *et al.* in a single layer graphene deposited on an oxide superconductor. [60] The comparatively easy way to measure the e-ph coupling constant with a HAS apparatus from the temperature dependence of the DW exponent could certainly facilitate the search for novel superconducting graphene systems.

When referring to graphene, an important remark is in order concerning the proportionality of λ_{HAS} to the temperature-dependent mean-square displacements entering the DW exponent, due to a persistent confusion in the literature between the perpendicularly-polarized acoustic ZA modes and the flexural modes. The ZA modes are solutions of a thin elastic plate with fixed boundaries or periodic boundary conditions, and their frequency is proportional to the wavevector in the long-wave limit, whereas, flexural modes are solutions for a thin elastic plate with free boundaries and have their frequency in the long-wave limit as proportional to the square of the wavevector. The difference is simply due to the fact that transverse deformations with fixed boundaries imply a longitudinal strain, whereas in flexural modes the boundaries can move and no strain occurs. The issue has been clarified between the late XVIII and early XIX centuries by the works of Euler, Bernoulli, DAlembert, Sophie Germain and Lagrange, just to mention the pioneers, and the terminology is well established. [17] What holds for graphene, is *a fortiori* valid for any self-standing layer structure. More details are given in the Supplementary Material (see appendix).

The difference between the ZA and flexural modes is particularly relevant for the DW factor because in a linear chain or a 2D lattice of N atoms with cyclic boundary conditions the mean-square displacement at a given temperature tends to a finite value for $N \rightarrow \infty$, whereas in a linear chain or 2D lattice with free boundaries the mean-square displacement of the flexural mode diverges for $N \rightarrow \infty$ at any temperature. [62, 63, 64, 65, 66, 67] Such large amplitude behavior has been reported on unsupported graphene as measured with high resolution electron microscopy. [68, 69, 70, 71] Moreover, exotic large amplitude vibrations at the free edges of suspended graphene ribbons, not predicted by classical homogeneous elastic plate dynamics, have been demonstrated by García-Sánchez *et al.* with a novel scanning probe microscopy method. [72] Considering that experiments on perfectly suspended graphene flakes with free boundaries, as well as first-principle calculations without imposing cyclic boundary conditions, are hard to carry out, the frequent assumption of a quadratic dispersion

for $\omega_{ZA}(\mathbf{Q})$, and the term *flexural* for the ZA mode, appear to be inappropriate.

On the other hand, finite flakes of weakly coupled (quasi-self-standing) supported graphene may approximate the free-boundary condition, thus yielding a mean-square displacement rapidly increasing with temperature, i.e., a steep decrease of the DW factor. In this case the association of DW slopes like those of Fig. 1a) exclusively to e-ph interaction may be incorrect, especially for the weakest graphene-substrate couplings.

5. Conclusions

To conclude, what has been demonstrated here is that a relatively simple measurement of the thermal attenuation of He atom diffraction can be used to extract values of the e-ph coupling constant $\lambda = \lambda_{HAS}$ for single layer graphene supported on close-packed metal substrates. This is an extension of previous work that determined λ_{HAS} for simple metal surfaces, and shows that the e-ph coupling constant can be determined for much more complicated surface systems. All available data for both He and Ne atom scattering from Gr/metals have been analyzed here, as well as data for clean graphite. A significant result arises when λ_{HAS} is plotted as a function of the spring constant f_{\perp} binding the graphene to the substrate: the weakly bonded systems have large values of λ_{HAS} while the strongly bonded systems have smaller values. In a plot of λ_{HAS} versus f_{\perp} all data points fall on a smooth curve according to the law $I_{HAS}(f_{\perp}) = I_{HAS}(0)/(1+f_{\perp}/f_D)$ with f_D the effective Debye force constant of graphene. This fit allows a very reasonable extrapolation to $f_{\perp} \rightarrow 0$, which makes the interesting prediction that a large, flat, free-standing sheet of graphene (obeying fixed or cyclic boundary conditions) with a free carrier concentration of the order of 10^{13} cm^{-2} , like the supported graphene systems considered here, should have an e-ph constant with the relatively large value of 0.89. It would be extremely interesting to verify it by carrying out He atom scattering experiments on unsupported graphene. The implications of this work suggest several additional experiments that would be of interest to carry out with He atom scattering on graphene and related systems. One such class of experiments would be to measure extensive energy-resolved inelastic scattering spectra. Such spectra exhibit peak-features due to specific phonons, and these peak intensities are directly proportional to $\lambda_{\mathbf{Q},\nu}$, the mode-selected e-ph contributions to λ_{HAS} . [15] Thus, inelastic atom-scattering can provide unique information on which phonon modes contribute most importantly to λ .

Another class of experiments would be to measure double and multiple layer supported graphene, and in particular it would be interesting to measure λ for twisted bilayer graphene (tBLG) which can be superconducting for specific twist angles, [73, 74, 75, 76] as well as measurements on the class of layered transition-metal chalcogenides which exhibit 2D superconductivity (see, e.g., the recent work by Trainer *et al.* [77] and the HAS study of 2H-MoS₂ [78]). In the specific case of tBLG, where its peculiar electronic structure is considered to favor a strong electron correlation as the basic mechanism for pairing, [73, 74, 75, 79, 80] the actual value of λ would be

rather small. On the other hand, it has been suggested that the very same electronic structure at the Fermi level supports a strong e-ph interaction with λ of the order of 1, [81, 82, 83, 84] or even 1.5, [85] so as to consider tBLG as a conventional superconductor. This would rely on a strong multivalley e-ph interaction as well as on a decoupling between twisted layers, similar to the orientational stacking faults in graphene multilayers grown on 4H-SiC(0001) which makes the surface layer behave as a self-standing doped graphene.[86] This may well correspond to the large λ in the limit $f_{\perp} \rightarrow 0$ represented in Fig. 2. Helium atom scattering on tBLG and twisted multilayer graphene would certainly help to clarify the above issue.

Acknowledgments: We would like to thank Profs. M. Bernasconi, P. M. Echenique, E. Chulkov and D. Farías for helpful discussions. This work is partially supported by a grant with Ref. FIS2017-83473-C2-1-P from the Ministerio de Ciencia (Spain).

- [1] Al Taleb A, Anemone G, Miranda R and Farías D 2018 Characterization of interlayer forces in 2D heterostructures using neutral atom scattering *2D Mater.* **5**, 045002.
- [2] Oh J P, Kondo T, Hatake D and Nakamura J 2009 Elastic and Inelastic Scattering Components in the Angular Intensity Distribution of He Scattered from Graphite *Surf. Sci.* **603**, 895.
- [3] Shichibe H, Satake Y, Watanabe K, Kinjyo A, Kunihara A, Yamada Y, Sasaki M, Hayes W W and Manson J R 2015 Probing interlayer interactions between graphene and metal substrates by supersonic rare-gas atom scattering *Phys. Rev. B* **91**, 155403.
- [4] Al Taleb A, Anemone G, Farías D and Miranda, R 2018 Resolving localized phonon modes on graphene/Ir(111) by inelastic atom scattering *Carbon* **133**, 31.
- [5] Gibson K D and Sibener S J 2016 Growth Structure, and Vibrational Properties of Few Layer Graphene Grown on Rh(111) *J. Phys. Chem. C* **120**, 24158.
- [6] Al Taleb A, Yu H K, Anemone G, Farías D and Wodtke A M 2015 Helium diffraction and acoustic phonons of graphene grown on copper foil *Carbon* **95**, 731.
- [7] Maccariello D, Campi D, Al Taleb A, Benedek G, Faras D, Bernasconi M and Miranda R 2015 Low-energy excitations of graphene on Ru(0001) *Carbon* **93**, 1.
- [8] Al Taleb A, Anemone G, Faras D and Miranda R 2016 Acoustic surface phonons of graphene on Ni(111) *Carbon* **99**, 416.
- [9] Anemone G, Al Taleb A, Hayes W W, Manson J R and Farías D 2017 Quantum Decoherence Behavior in Neon Scattering from Ru(0001) and Graphene/Ru(0001) Surfaces: Experiment and Comparison with Calculations *J. Phys. Chem. C* **121**, 22815.
- [10] Politano A, Borca B, Minniti M, Hinarejos J J, Vázquez de Parga A L, Farías D and Miranda, R 2011 Helium Reflectivity and Debye Temperature of Graphene Grown Epitaxially on Ru(0001) *Phys. Rev. B* **84**, 35450.
- [11] Al Taleb A, Anemone G, Hayes W W, Manson J R and Farías D 2017 Multiphonon excitation and quantum decoherence in neon scattering from solid surfaces *Phys. Rev. B* **95**, 075414.
- [12] Tamtögl A, Bahn E, Zhu J, Fouquet P, Ellis J and Allison W 2015 Graphene on Ni(111): Electronic Corrugation and Dynamics from Helium Atom Scattering *J. Phys. Chem. C* **119**, 25983.
- [13] Allen P B 1972 Neutron Spectroscopy of Superconductors *Phys. Rev. B* **6**, 2577.
- [14] Sklyadneva I Yu, Benedek G, Chulkov E V, Echenique P M, Heid R, Bohnen K-P and Toennies J P 2011 Mode-Selected Electron-Phonon Coupling in Superconducting Pb Nanofilms Determined

from He Atom Scattering *Phys. Rev. Lett.* **107**, 095502.

[15] Benedek G, Bernasconi M, Bohnen K-P, Campi D, Chulkov E V, Echenique P M, Heid R, Sklyadneva I Yu and Toennies J P 2014 Unveiling mode-selected electron-phonon interactions in metal films by helium atom scattering *Phys. Chem. Chem. Phys.* **16**, 7159.

[16] Manson J R, Benedek G and Miret-Artés S 2016 Electron-phonon coupling strength at metal surfaces directly determined from the helium atom scattering Debye-Waller factor *J. Phys. Chem. Lett.* **7**, 1016; *ibid.* **7**, 1691.

[17] Benedek G, Miret-Artés S, Toennies J P and Manson J R 2018 The electron-phonon coupling constant of metallic overlayers from specular He-atom scattering *J. Phys. Chem. Lett.* **9**, 76.

[18] Manson J R, Benedek G and Miret-Artés S Atom scattering as a probe of the surface electron-phonon interaction *Surface Science Reports*, unpublished.

[19] Benedek G; Miret-Artés S, Manson J R, Ruckhofer A, Ernst W E and Tamtögl A 2020 Origin of the Electron-Phonon Interaction of Topological Semimetal Surfaces Measured with Helium Atom Scattering *J. Phys. Chem. Lett.* **11**, 1927.

[20] Hoinkes H 1980 The physical interaction potential of gas atoms with single-crystal surfaces, determined from gas-surface diffraction experiments *Rev. Mod. Phys.* **52**, 933.

[21] Benedek G and Toennies J P 2018 Atomic Scale Dynamics at Surfaces: Theory and Experimental Studies with Helium Atom Scattering *Springer Series in Surface Sciences*, **63** (Springer Press, Heidelberg) ISBN 978-3-662-56443-1.

[22] Hulpke E (Ed.) 1992 Helium Atom Scattering from Surfaces *Springer Series in Surface Sciences* **27** (Springer Press, Heidelberg).

[23] Farias D and Rieder K-H 1998 Atomic beam diffraction from solid surfaces *Rep. Prog. Phys.* **61**, 1575.

[24] Giovannetti G, Khomyakov P A, Brocks G, Karpan V M, van den Brink J and Kelly P J 2008 Doping Graphene with Metal Contacts *Phys. Rev. Lett.* **101**, 026803.

[25] Vita H, Bottcher S, Horn K, Voloshina E N, Ovcharenko R E, Kampen T, Thissen A and Dedkov Y S 2014 Understanding the origin of band gap formation in graphene on metals: graphene on Cu/Ir(111) *Sci. Rep.* **4**, 5704.

[26] Sutter P, Sadowsky J T and Sutter E 2009 Graphene on Pt(111): Growth and substrate interaction *Phys. Rev. B* **80**, 245411.

[27] Alattas M and Schwingenschlögl U 2016 Quasi-freestanding graphene on Ni(111) by Cs intercalation *Sci. Rep.* **6**, 26753.

[28] Katsiev K, Losovyj Y, Zhou Z H, Vescovo E, Liu L, Dowben P A and Goodman D W 2012 Graphene on Ru(0001): Evidence for two graphene band structures *Phys. Rev. B* **85**, 195405.

[29] Walter A L, Nie S, Bostwick A, Kim K S, Moreschini L, Chang Y J, Innocenti D, Horn K, McCarty K F and Rotenberg E 2011 Electronic structure of graphene on single-crystal copper substrates *Phys. Rev. B* **84** 195443.

[30] Ariel V, and Natan N, arXiv: 1206.6100v2 [physics.gen-ph] 12 Aug 2012; and 2013 Int. Conf. on Electromagnetics in Advanced Applications (ICEAA), 696-698, doi: 10.1109/ICEAA.2013.663234.

[31] Fedorov A V, Verbitskiy N I, Haberer D, Struzzi C, Petaccia L, Usachov D, Vilkov O Y, Vyalikh D V, Fink J, Knupfer M, Büchner B and Grüneis A 2014 Observation of a universal donor-dependent vibrational mode in graphene *Nat. Commun.* **5**, 3257.

[32] Park C-H, Giustino F, Cohen M L and Louie S G 2008 Electron-Phonon Interactions in Graphene, Bilayer Graphene, and Graphite *Nano Lett.* **8**, 4229.

[33] Kelly M J and Falicov L M 1977 Electronic Ground-State of Inversion Layers in Many-Valley Semiconductors *Phys. Rev. B* **15**, 1974.

[34] Kelly M J and Falicov L M 1977 Optical-Properties of Charge-Density-Wave ground-States for Inversion Layers in Many-Valley Semiconductors *Phys. Rev. B* **15**, 1983.

[35] Kelly M J and Falicov L M 1976 Electronic Structure of Inversion Layers in Many-Valley Semiconductors *Phys. Rev. Lett.* **37**, 1021.

- [36] Vollmer R 1992 Ph. D. Thesis, University of Göttingen, p. 140.
- [37] Bailey A C and Yates B 1970 Anisotropic thermal expansion of pyrolytic graphite at low temperature. *J. Appl. Phys.* **41**, 5088.
- [38] Marsden B, Mummery A and Mummery P. 2018 Modelling the coefficient of thermal expansion in graphite crystals: implications of lattice strain due to irradiation and pressure *Proc. Roy. Soc. A* **474**, 0075; and references therein.
- [39] Bose S K, Dolgov O V, Kortus J, Jepsen O and Andersen O K 2002 Pressure dependence of electron-phonon coupling and superconductivity in hcp Fe: A linear response study *Phys. Rev. B* **67**, 214518.
- [40] Mounet N and Marzari N 2005 First-principles determination of the structural, vibrational and thermodynamic properties of diamond, graphite, and derivatives *Phys. Rev. B* **71**, 205214.
- [41] Al Taleb A and Farías D 2016 Phonon dynamics of graphene on metals *J. Phys.: Condens. Matter* **28**, 103005.
- [42] McMillan W L 1968 Transition Temperature of Strong-Coupled Superconductors *Phys. Rev.* **167**, 331.
- [43] Grimvall G 1981 The Electron-Phonon Interaction in Metals (North-Holland, New York).
- [44] Michaelson H B 1977 Work Function of Elements and its Periodicity *J. App. Phys.* **48**, 4729.
- [45] Poole C P, Zasadinsky J F, Zasadinsky R K and Allen P B 1999 Electron-phonon coupling constants, in Handbook of Superconductivity C. P. Poole, Jr. ed. (Academic Press, New York) Ch. 9, Sec. G, pp. 478-483.
- [46] Allen P B 1987 Empirical electron-phonon-gamma values from resistivity of cubic metallic elements *Phys. Rev. B* **36**, 2920.
- [47] Shen X, Timalsina Y P, Lu T-M and Yamaguchi M 2015 Experimental study of electron-phonon coupling and electron internal thermalization in epitaxially grown ultrathin copper films *Phys. Rev. B* **91**, 045129.
- [48] Sugawara K, Sato T, Souma S, Takahashi T and Suematsu H 2007 Anomalous Quasiparticle Lifetime and Strong Electron-Phonon Coupling in Graphite *Phys. Rev. Lett.* **98**, 036801; ARPES measurements in K-K direction.
- [49] Moos G, Gahl C, Fasel R, Wolf M and Tobias Hertel T 2002 Anisotropy of Quasiparticle Lifetimes and the Role of Disorder in Graphite from Ultrafast Time-Resolved Photoemission Spectroscopy *Phys. Rev. Lett.* **87**, 267402.
- [50] Leem C S, Kim B J, Kim C, Park S R, Ohta T, Bostwick A, Rotenberg E, Kim H-D, Kim M K, Choi H J and Kim C 2008 Effect of Linear Density of States on the Quasiparticle Dynamics and Small Electron-Phonon Coupling in Graphite *Phys. Rev. Lett.* **100**, 016802.
- [51] Politano A, Marino A R and Chiarello G 2012 Phonon-dispersion of quasi-freestanding graphene on Pt(111) *J. Phys.: Condens. Matter* **24**, 104025.
- [52] Wu M-Ch, Xu Q and Goodman D W 1994 Investigations of Graphitic Overlayers Formed from Methane Decomposition on Ru(0001) and Ru(1120) Catalysts with Scanning Tunneling Microscopy and High-Resolution Electron Energy Loss Spectroscopy *J. Phys. Chem.* **98**, 5104.
- [53] Braun J, Kostov K L, Witte G, Surnev L, Skofronick J G, Safron S A and Wöll Ch 1997 Surface phonon dispersion curves for a hexagonally close packed metal surface: Ru(0001) *Surf. Sci.* **372**, 132.
- [54] Heid R, Bohnen K-P, Moritz T, Kostov K L, Menzel D and Widdra W 2002 Anomalous surface lattice dynamics of a simple hexagonal close-packed surface *Phys. Rev. B* **66**, 161406.
- [55] Zhou J, Sun Q, Wang Q and Jena P 2015 High-temperature superconductivity in heavily N- or B-doped graphene *Phys. Rev. B* **92**, 064505.
- [56] Larkins G, Vlasov Y and Holland K 2016 Evidence of superconductivity in doped graphite and graphene *Supercond. Sci. Technol.* **29**, 015015.
- [57] Yang S L, Sobota J A, Howard C A, Pickard C J, Hashimoto M, Lu D H, Mo S K, Kirchmann P S and Shen Z X 2014 Superconducting graphene sheets in CaC₆ enabled by phonon-mediated interband interactions. *Nat. Commun.* **5**, 3493.

- [58] Chapman J, Su Y, Howard C A, Kundys D, Grigorenko A N, Guinea F, Geim A K, Grigorieva I V and Nair R R 2016 Superconductivity in Ca-doped graphene laminates, *Scientific Reports* **6**, 23254.
- [59] Profeta G, Calandra M and Mauri F 2012 Phonon-mediated superconductivity in graphene by lithium deposition *Nat. Phys.* **8**, 131.
- [60] Di Bernardo A, Millo O, Barbone M, Alpern H, Kalcheim Y, Sassi U, Ott A K, De Fazio D, Yoon D, Amado M, Ferrari A C, Linder J and Robinson J W A 2017 p-wave triggered superconductivity in single-layer graphene on an electron-doped oxide superconductor *Nat. Comm.* **8**, 14024.
- [61] For a review and historical references, see: Szilard R 2004 Theories and Applications of Plate Analysis - Classical, Numerical and Engineering Methods, (John Wiley and Sons, Inc., New York).
- [62] Peierls R E 1934 Bemerkungen über Umwandlungstemperaturen *Helv. Phys. Acta* **7**, 81.
- [63] Peierls R E 1935 Quelques propriétés typiques des corps solides *Ann. Inst. Henri Poincaré* **5**, 177.
- [64] Landau L D 1937 Zur Theorie der Phasenumwandlungen II *Phys. Z. Sowjetunion* **11** 26.
- [65] Landau L D and Lifshitz E M 1980 Statistical Physics Part I (Pergamon, Oxford), Sections 137 and 138.
- [66] Mermin N D and Wagner H 1966 Absence of ferromagnetism or antiferromagnetism in one- or two-dimensional isotropic Heisenberg models *Phys. Rev. Lett.* **17**, 1133.
- [67] Mermin N D 1968 Crystalline Order in Two Dimensions *Phys. Rev.* **176**, 250.
- [68] Meyer J C, Geim A K, Katsnelson M I, Novoselov K S, Booth T J and Roth S 2007 The structure of suspended graphene sheets *Nature* **446**, 60.
- [69] Meyer J C, Geim A K, Katsnelson M I, Novoselov K S, Obergfell D, Roth S, Girit C and Zettl A 2007 On the roughness of single- and bi-layer graphene membranes *Solid State Communications* **143**, 101.
- [70] Brivio J, Alexander D T L and Kis A 2011 Ripples and Layers in Ultrathin MoS₂ Membranes *Nano Lett.* **11**, 5148.
- [71] Kirilenko D A, Dideykin A T and Van Tendeloo G 2011 Measuring the corrugation amplitude of suspended and supported graphene *Phys. Rev. B* **84**, 235417.
- [72] Garca-Sanchez D, van der Zande A M, San Paulo A, Lassagne B, McEuen P L and Bachtold A 2008 Imaging mechanical vibrations in suspended graphene sheets. *Nano Lett.* **8**, 1399.
- [73] Bistritzer R and MacDonald A H 2011 Moiré bands in twisted double.layer graphene 2011 *Proc. Nat. Acad. Sci.* **108**, 12233.
- [74] Cao Y, Fatemi V, Fang S, Watanabe K, Taniguchi T, Kaxiras E and Jarillo-Herrero P 2018 Unconventional superconductivity in magic-angle graphene superlattices *Nature* **556**, 43.
- [75] Cao Y, Fatemi V, Demir A, Fang S, Tomarken S L, Luo J Y, Sanchez-Yamagishi J D, Watanabe K, Taniguchi T, Kaxiras E, Ashoori R C and Jarillo-Herrero P 2018 Correlated insulator behaviour at half-filling in magic-angle graphene superlattices *Nature* **556**, 80.
- [76] Mogera U and Kulkarni G U 2020 A new twist in graphene research: Twisted graphene *Carbon* **156**, 470.
- [77] Trainer D J, Wang B, Bobba F, Samuelson N, Xi X, Zasadzinski J, Nieminen J, Bansil A and Iavarone M 2020 Proximity-induced superconductivity in monolayer MoS₂ *ACS Nano* **14**, 2718.
- [78] Anemone G, Al Taleb A, Benedek G, Castellanos-Gomez A and Farías D, Electron-Phonon Coupling Constant of MoS₂, 2019, *J. Phys. Chem. C* **123**, 3682.
- [79] Liu C-C, Zhang L-D, Chen W-Q and Yang F 2018 Chiral spin density Wave and d + id superconductivity in the magic-angle-twisted bilayer graphene *Phys. Rev. Lett.* **121**, 217001.
- [80] Yankowitz M, Chen S, Polshyn H, Zhang Y, Watanabe K, Taniguchi T, Graf D, Young A F and Dean C R 2019 Tuning superconductivity in twisted bilayer graphene *Science* **363**, 1059.
- [81] Wu F, MacDonald A H and Martin I 2018 Theory of phonon-mediated superconductivity in twisted bilayer graphene *Phys. Rev. Lett.* **121**, 217001.

- [82] Choi Y W and Choi H J 2018 Electron-phonon interaction in magic-angle twisted bilayer graphene *Phys. Rev. B* **98**, 241412.
- [83] Sarma S D and Wu F 2019 Electron-phonon and electron-electron interaction effects in twisted bilayer graphene. arXiv:1910.08556v1 [cond-mat.mes-hall].
- [84] Wu F, Hwang E and Sarma S D 2019 Phonon-induced giant linear-in-T resistivity in magic angle twisted bilayer graphene: Ordinary strangeness and exotic superconductivity *Phys. Rev. B* **99**, 165112.
- [85] Lian B, Wang Z and Bernevig B A 2019 Twisted Bilayer Graphene: A Phonon-Driven Superconductor *Phys. Rev. Lett.* **122**, 257002.
- [86] Hass J, Varchon F, Milln-Otoya J E, Sprinkle M, Sharma N, de Heer W A, Berger C, First P N, Magaud L and Conrad E H 2008 Why multilayer graphene on 4H-SiC(0001) behaves like a single sheet of graphene *Phys. Rev. Lett.* **100**, 125504.

Appendix A: Supplemental Material: The Electron-Phonon Coupling Constant for Single-Layer Graphene on Metal Substrates Determined from He Atom Scattering

Comparison of ZA and flexural phonon modes

In the context of measuring the electron-phonon constant, it is of interest to discuss the unique phonon modes added to the semi-infinite bulk when graphene is adsorbed onto the metal substrate. A free-standing (unsupported) sheet of graphene has three acoustic phonon branches, one with a longitudinal (LA) and two with transverse polarization, one in-plane [shear horizontal, (SH)] and one normal to the plane [shear vertical, (SV) or sometimes denoted as (ZA)]. By imposing cyclic boundary conditions as well as translational and rotational invariance conditions the three branches have a linear dispersion for $\mathbf{Q} \rightarrow 0$ corresponding to three distinct speeds of sound. When adsorbed to a substrate, the three modes lose their linear dispersion and at small parallel wave vector \mathbf{Q} their frequencies go to finite values $\omega_j(0)$ ($j = \text{ZA, SH, LA}$) due to the bonding force constants between the graphene and the substrate. Since for ZA modes the bonding force constant is essentially radial, while those for LA and SH modes are mostly transverse, in general $\omega_{ZA}(0) > \omega_{LA}(0) > \omega_{SH}(0)$. The experimental $\omega_{ZA}(0)$, or better the corresponding bonding force constant f_\perp can be taken as a measure of the graphene-substrate interaction. For a free-standing infinite-extent thin membrane, such as graphene, the dispersion relation for the ZA mode exhibits a typical upward curvature due to the sp^2 bonding structure and consequent strong angle-bending forces, and can be approximated by [1, 2, 3]

$$\omega_{ZA}^2(\mathbf{Q}) = v_{SV}^2 \mathbf{Q}^2 + \frac{\kappa}{\rho_{2D}} \mathbf{Q}^4, \quad (1)$$

where v_{SV} is the speed of SV waves, κ is the bending rigidity (sometimes called the flexural rigidity), and ρ_{2D} is the 2-D mass density. However, if the membrane is coupled to the substrate, the coupling force constant will introduce a gap of frequency $\omega_{ZA}(0)$. In this case the corresponding dispersion in the region of small \mathbf{Q} is often expressed as [4]

$$\omega_{ZA}^2(\mathbf{Q}) = \omega_{ZA}^2(0) + \frac{\kappa}{\rho_{2D}} \mathbf{Q}^4, \quad (2)$$

written without the quadratic term, its effect being negligible with respect to that of the other two terms. It is Eq. (2) that has been used to determine the bending rigidity κ of the ZA mode of graphene supported by the metals considered here [5, 6, 7, 8, 9] as well as for the thinnest known layer of vitreous glass, a bilayer of SiO_2 on $\text{Ru}(0001)$. [10]

It is important to note that most of the modelling of supported graphene dynamics is based on the assumption of a rigid substrate. However, the phonon spectrum of graphene, with its large dispersion of acoustic modes and high-frequency optical modes,

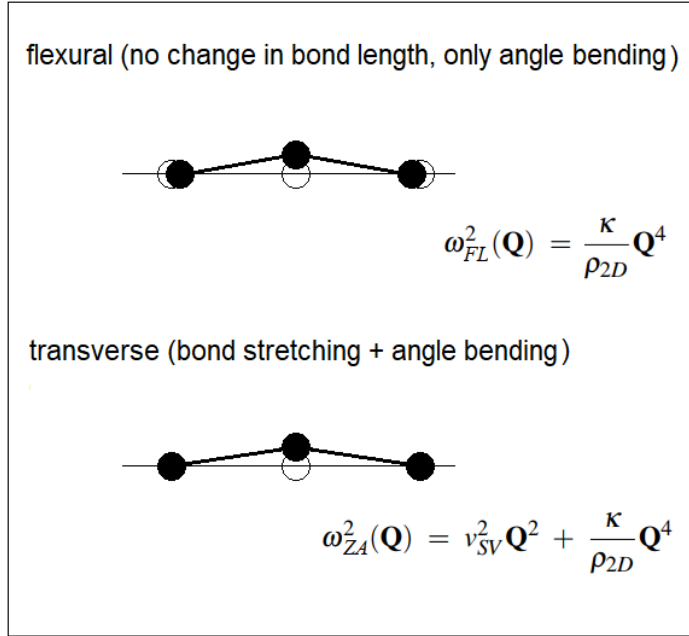


Figure 1. Angle bending displacement patterns in a linear chain for a flexural (FL) mode (above) and a shear-vertical (SV) transverse mode (below, also called the ZA mode), with the equations of the respective dispersion relations. While the SV mode fulfills cyclic boundary conditions, which implies bond stretching, the FL mode does not and is only allowed by free boundary conditions.

covers the whole phonon spectrum of the substrate, and therefore several avoided crossings are expected between graphene and the substrate modes of similar polarization. For the ZA branch the important interactions are with the S_2 optical branch of the metal and the Rayleigh wave. For this reason it was convenient to replace the carbon dimer mass with the effective mass in the expression of f_\perp used in Fig. 2 of the manuscript. Moreover, supported graphene is no longer a specular plane, and coupled SV phonon modes acquire some elliptical polarization, leading, e.g., to an avoided crossing between the ZA and LA modes near $\mathbf{Q} = 0$ (see, for example, HAS data for Gr/Ru(0001) [8]).

In recent works on free-standing graphene dynamics (and even on graphite dynamics) there is some apparent confusion between SV transverse (ZA) and flexural modes. [7, 11, 12, 13, 14, 15] This also appears in the case of other thin film materials such as bilayer SiO₂. [10, 16] The study of the dynamics of elastic plates dates back to works of Euler, Bernoulli, D'Alembert, Sophie Germain and Lagrange, just to mention some of the pioneers, and the terminology is well established. [17] When transferred to lattice dynamics, transverse modes refer to lattices with cyclic (or fixed) boundary conditions, whereas flexural modes refer to lattices with free boundaries. The difference is illustrated for a three-atom chain in Fig. 1. The flexural mode, where angle bending occurs with no change of the bond lengths, clearly does not fulfill cyclic boundary conditions, and the frequency dispersion is not linear for $\mathbf{Q} \rightarrow 0$, but is quadratic. On the other hand, in the transverse ZA mode angle bending occurs with bond stretching

in order to fulfill the boundary conditions, and the frequency dispersion is linear for $\mathbf{Q} \rightarrow 0$.

- [1] Landau L D and Lifshitz I M 1986 Theory of Elasticity, Third Edition, (Elsevier, Amsterdam), Section 25.
- [2] Nihira T and Iwata T 2003 Temperature dependence of lattice vibrations and analysis of the specific heat of graphite. *Phys. Rev. B* **68**, 134305.
- [3] Nika D L and Balandin A A 2017 Phonons and thermal transport in graphene *Rep. Prog. Phys.* **80**, 036502.
- [4] Amorim B and Guinea F 2013 Flexural mode of graphene on a substrate *Phys. Rev. B* **88**, 115418.
- [5] Al Taleb A, Anemone G, Farías D and Miranda, R 2018 Resolving localized phonon modes on graphene/Ir(111) by inelastic atom scattering *Carbon* **133**, 31.
- [6] Gibson K D and Sibener S J 2016 Growth Structure, and Vibrational Properties of Few Layer Graphene Grown on Rh(111) *J. Phys. Chem. C* **120**, 24158.
- [7] Al Taleb A, Yu H K, Anemone G, Farías D and Wodtke 2015 A M Helium diffraction and acoustic phonons of graphene grown on copper foil *Carbon* **95**, 731.
- [8] Maccariello D, Campi D, Al Taleb A, Benedek G, Faras D, Bernasconi M and Miranda R 2015 Low-energy excitations of graphene on Ru(0001) *Carbon* **93**, 1.
- [9] Al Taleb A, Anemone G, Faras D and Miranda R 2016 Acoustic surface phonons of graphene on Ni(111) *Carbon* **99**, 416.
- [10] Buchner C, Eder S D, Nesse T, Kuhness D, Schlexer P, Pacchioni G, Manson J R, Heyde M, Holst B and Freund H-J 2018 Bending Rigidity of 2D Silica *Phys. Rev. Lett.* **120**, 226101.
- [11] Saito R, Dresselhaus G and Dresselhaus M S 1998 Physical properties of carbon nanotubes. (Imperial College Press, London); Chapter 9.
- [12] Castro Neto A H, Guinea F, Peres N M R, Novoselov K S and Geim A K 2009 The electronic properties of graphene *Rev. Mod. Phys.* **81**, 109.
- [13] Wirtz L and Rubio A 2004 The phonon dispersion of graphite revisited *Solid State Communications* **131**, 141.
- [14] Karssemeijer L J and Fasolino A 2011 Phonons of graphene and graphitic materials derived from the empirical potential LCBOPII *Surf. Sci.* **605**, 1611.
- [15] Liu D, Every A G and Tománek D 2016 Continuum approach for long-wavelength acoustic phonons in quasi-two-dimensional structures *Phys. Rev. B* **94**, 165432.
- [16] Gao E, Xie B and Xu Z 2016 Two-dimensional silica: Structural, mechanical properties, and strain-induced band gap tuning *J. App. Phys.* **119**, 014301.
- [17] For a review and historical references, see: Szilard R 2004 Theories and Applications of Plate Analysis - Classical, Numerical and Engineering Methods, (John Wiley and Sons, Inc., New York).